九州大学学術情報リポジトリ
Kyushu University Institutional Repository

Calculation of strained BaTiO3 with different exchange correlation functionals examined with criterion by Ginzburg-Landau theory, uncovering expressions by crystallographic parameters

Watanabe, Yukio
Department of Physics, Kyushu University

https://hdl.handle.net/2324/1929770

出版情報：The Journal of Chemical Physics. 148 (194702), pp.194702-1-194702-15, 2018-05-17.
AIP Publishing
バージョン：
権利関係：

Calculation of strained $BaTiO_3$ with different exchange correlation functionals examined with criterion by Ginzburg-Landau theory, uncovering expressions by crystallographic parameters

Yukio Watanabe

Citation: The Journal of Chemical Physics **148**, 194702 (2018); doi: 10.1063/1.5022319
View online: https://doi.org/10.1063/1.5022319
View Table of Contents: http://aip.scitation.org/toc/jcp/148/19
Published by the American Institute of Physics

PHYSICS TODAY
WHITEPAPERS
ADVANCED LIGHT CURE ADHESIVES
Take a closer look at what these environmentally friendly adhesive systems can do
READ NOW
PRESENTED BY
MASTERBOND
ADHESIVES | SEALANTS | COATINGS

Calculation of strained $BaTiO_3$ with different exchange correlation functionals examined with criterion by Ginzburg-Landau theory, uncovering expressions by crystallographic parameters

Yukio Watanabe
Department of Physics, Kyushu University, Fukuoka 819-0395, Japan

(Received 13 January 2018; accepted 18 April 2018; published online 17 May 2018)

In the calculations of tetragonal $BaTiO_3$, some exchange-correlation (XC) energy functionals such as local density approximation (LDA) have shown good agreement with experiments at room temperature (RT), e.g., spontaneous polarization (P_S), and superiority compared with other XC functionals. This is due to the error compensation of the RT effect and, hence, will be ineffective in the heavily strained case such as domain boundaries. Here, ferroelectrics under large strain at RT are approximated as those at 0 K because the strain effect surpasses the RT effects. To find effective XC energy functionals for strained $BaTiO_3$, we propose a new comparison, i.e., a criterion. This criterion is the properties at 0 K given by the Ginzburg-Landau (GL) theory because GL theory is a thermodynamic description of experiments working under the same symmetry-constraints as *ab initio* calculations. With this criterion, we examine LDA, generalized gradient approximations (GGA), meta-GGA, meta-GGA + local correlation potential (U), and hybrid functionals, which reveals the high accuracy of some XC functionals superior to XC functionals that have been regarded as accurate. This result is examined directly by the calculations of homogenously strained tetragonal $BaTiO_3$, confirming the validity of the new criterion. In addition, the data points of theoretical P_S vs. certain crystallographic parameters calculated with different XC functionals are found to lie on a single curve, despite their wide variations. Regarding these theoretical data points as corresponding to the experimental results, analytical expressions of the local P_S using crystallographic parameters are uncovered. These expressions show the primary origin of $BaTiO_3$ ferroelectricity as oxygen displacements. Elastic compliance and electrostrictive coefficients are estimated. For the comparison of strained results, we show that the effective critical temperature T_C under strain <-0.01 is >1000 K from an approximate method combining *ab initio* results with GL theory. In addition, in a definite manner, the present results show much more enhanced ferroelectricity at large strain than the previous reports. *Published by AIP Publishing.* https://doi.org/10.1063/1.5022319

I. INTRODUCTION

Ferroelectric materials have an electrically reversible spontaneous polarization P_S below a critical temperature T_C. Efforts to enhance their performance and extend the scope of their applications have been intensively pursued.[1] To pursue these aims from an atomic-scale perspective, *ab initio* calculations[2–10] are widely used. Here, the accuracies of the lattice constants and the mechanical properties are far more critical than for other materials.[10,11]

For many ferroelectric oxides, ferroelectric phases arise from tiny atomic distortions.[10,11] A representative parameter of the distortion of the prototypical ferroelectric $BaTiO_3$ is the ratio of the c- and a-axis lattice constant c/a. For example, the difference in the c/a ratio between the cubic paraelectric phase and the tetragonal ferroelectric phase of $BaTiO_3$ is only 1% at room temperature (RT).[12,13] For an incipient ferroelectric $SrTiO_3$,[14] a c/a ratio difference of 0.2% is significant.[15–17]

Because of such sensitivity of the ferroelectricity to the structure, accurate estimation of the distortions caused by mechanical stress or strain is important for the domains, epitaxial films, and miniaturized ferroelectrics. Here, the domains are P_S-aligned regions and 90° (ac) and antiparallel (180° or cc) domains are considered to originate from the mechanical stress and the macroscopic electric field, respectively.[1] An electric field emerging from an insufficiently screened P_S is referred to as a depolarization field, which is essential in theories on the vortex-type domain and the standard model of the cc domain (Kittel model).[1,18] The calculations of these domains are expected to critically depend on the accuracy of the internal force estimates given by *ab initio* calculations. In addition, the depolarization field has been considered as the cause of the failure to detect ferroelectricity in miniaturized ferroelectrics[19–21] and the formation of nanodomains.[20] On the other hand, the possibility of substantial intrinsic screening of the depolarization field is proposed,[22–25] which relaxes these instabilities and restrictions.[24]

For these problems, the accurate calculation of internal forces is of primary importance. Wahl *et al.* argued that the use of the experimental lattice constants in *ab initio* calculations is inappropriate[11] because it induces an external fictitious pressure on the system's unit cell. In practice, the experimental lattice constants of each unit cell are unknown in inhomogeneous situations such as domains.

To perform these calculations accurately, the choice of suitable *ab initio* methods such as functionals of the exchange-correlation (XC) energy, which is a key part of the density functional theory (DFT), is crucial[10,11,26,27] but is hindered by an obstacle. Specifically, the lattice symmetry of the equilibrium phase at 0 K of $BaTiO_3$ and many other ferroelectric oxides is different from that at RT, whereas *ab initio* calculations are generally for 0 K. For example, benchmark tests of *ab initio* calculations of ferroelectrics are mostly comparisons between calculations for 0 K and experiments at RT for stress-free cases,[10,11,26,27] with the notable exception of $PbTiO_3$.[28] Here, $BaTiO_3$ and $SrTiO_3$ have special significance for theoretical comparisons due to the critical dependence of the experimental values on sample quality[12,13] and the availability of many reports of experiments using high-quality single crystals. For example, the high quality of these crystals is evidenced in the high transparency used in electro-optics and the observations of the negative carrier type (*n*-type) conduction by oxygen vacancy.[29,30] On the other hand, in $PbTiO_3$, positive carrier type (*p*-type) is observed due to the volatility of PbO.[29,30]

Benchmark tests of functionals of the XC energy (XC functionals) for stress-free ferroelectrics[10,11,26,27] have shown that properties critically depend on them; in a conventional criterion that is the comparison with the RT experiments, some XC functionals, such as the standard versions of the generalized gradient approximation (GGA) and hybrid functionals, overestimate the *c*/*a* ratio and P_S.[10,26] These tests have also shown that some XC functionals[9,10] such as local density approximation (LDA) predict values of *c*/*a* ratio and P_S that are close to the experimental results at RT and, therefore, are considered reasonable choices.

However, accurate comparisons should be those between experiments at 0 K and *ab initio* calculations. The present paper reports such comparisons proposing a *new criterion*, which is the comparison with the properties at 0 K of the RT-phase given by the Ginzburg-Landau (GL) theory.[31–33]

The direct calculations of the domains and depolarization field are unsuitable as tests of the accuracy of internal forces. This is because these subjects are unsettled[34] and the calculation of domains usually requires molecular dynamics (MD) simulations that are less accurate than standard *ab initio* calculations. On the other hand, ferroelectricity under external strain, where the magnitude is comparable with those of these situations, has been experimentally established.[16,31] Indeed, the strain-enhancement of T_C and P_S has been known for over half a century[16,31,35,36] and is self-evident from the GL theory when limited to tetragonal (*P*4*mm*) ferroelectrics (Sec. III).[20,24,31] To date, strain effects have also been studied using *ab initio* calculations since at least 1998,[37–41] using LDA.

In contrast to conventional views, the new criterion proposed here reveals the advantages of some XC functionals over those of the XC functionals that have been considered accurate. The same conclusion was obtained by the direct calculations of the homogeneous strain effect, which shows the reliability of the new criterion and the rating of XC functionals for tetragonal $BaTiO_3$. These GL values and the methods employed here can also be used for examinations of other *ab initio* calculations. A similar study on $SrTiO_3$ reports that the choice of XC functionals causes a 10-fold difference in the critical strain for ferroelectricity.[42]

Ab initio calculations of P_S with a specific XC functional deviate from the real values in a specific manner. We found that the deviations were mainly due to crystallographic parameters. Assuming that experimental situation corresponding to these deviations exists, we found excellent correlations between the P_S and the crystallographic parameters from their theoretical sets. This yielded analytical expressions of P_S with lattice parameters. These examinations will show that (1) the oxygen position is more appropriate than the Ti position as an identifier of P_S and (2) the distance between Ti and O is the primary order parameter.

This paper is organized as follows: Sec. II describes the technical details of our calculations and briefly introduces DFT+*U* and hybrid functional. Section III derives GL theory for tetragonal phases under biaxial strain. Its validity is tested with published experimental data. Section IV describes the tests of *ab initio* calculations with available XC functionals for stress-free $BaTiO_3$, which are compared with GL estimates and available experiments. Section V reports the *ab initio* results of the tetragonal phase of $BaTiO_3$ under biaxial strain. Section VI reports analytical expressions of P_S by lattice parameters. Section VII discusses implications of the present results. Section VIII summarizes the results.

II. TECHNICAL DETAILS OF *AB INITIO*

$BaTiO_3$ is cubic at temperature above T_C and tetragonal at RT that is space group symmetry *P*4*mm*. We use LDA, Perdew-Burke-Ernzerhof (PBE) functional,[3] and PBE for solids (PBEsol)[4] as GGA, Tao-Perdew-Staroverov-Scuseria (TPSS) functional as meta-GGA,[5,6] and Heyd-Scuseria-Ernzerhof (HSE) functional[7] and HSE for solid (HSEsol) as hybrid functionals.[8] LDA, GGA, and meta-GGA functionals are functionals of the local electron density, the local electron density and its 1st spatial derivative, and the local electron density and its 1st and 2nd spatial derivatives, respectively. Hybrid functionals are mixtures of Hartree-Fock and DFT. In addition, DFT+*U* methods[43] are tested. Here, the results only by TPSS+*U* will be reported because this combination agreed best with experiments of stress-free $BaTiO_3$.

PBEsol is a PBE modified for solid by replacing the values of two scaling coefficients.[4] In HSE, a screened Coulomb potential hybrid density functional is constructed from a short and a long-range exchange term.[7] HSEsol is the same as HSE except for the use of PBSsol instead of PBE.[8] In the present paper, HSE means a revised version of HSE (HSE06),[44] and screening length μ is the default value (0.2 $Å^{-1}$),[7,8] while Wahl *et al.* used 0.3 $Å^{-1}$.[11]

The DFT+*U* method adds a Hubbard-like term to the total energy functional, to remedy the lack of electron localization. This method effectively adds an on-site Coulomb interaction term *U* inside each atomic sphere to DFT functionals, where *U* is given empirically or by other calculations. For stress-free $BaTiO_3$, both Liechtenstein and Dudarev schemes for

DFT+U[45,46] without exchange term ($J = 0$) yielded mutually similar results. Therefore, the present paper reports the results with the Liechtenstein scheme with $J = 0$.

All calculations were performed using the project augmented wave (PAW) method[47] as implemented in the Vienna *ab initio* simulation package (Vasp)[48] with a plane wave energy cutoff of 650 eV. PAW potentials are chosen from those supplied by Vasp so that the calculations with each XC functional agree best with stress-free $BaTiO_3$. For the Brillouin-zone integration, a Monkhorst-Pack mesh[49] of $6 \times 6 \times 6$ was used in geometry relaxation and Berry phase calculation of P_S.[50,51] In the calculations of biaxially strained $BaTiO_3$, geometry is fully relaxed under the constraint of fixed values of the a-axis lattice constant. After the geometry relaxations, all the calculated forces are always less than 0.001 eV/Å. These results were the same for denser mesh with lower calculated forces. The effects of different PAW potentials and the screening length of HSE and HSEsol were much smaller than the difference of XC functionals.

Wahl *et al.* calculated *stress-free* $BaTiO_3$.[11] The present PBEsol results for *stress-free* $BaTiO_3$ agree completely with those of Wahl *et al.*[11] including the zone-center phonon frequencies. In addition, the present results by LDA, PBE, and HSE for *stress-free* $BaTiO_3$ agree well with those of Wahl *et al.* including the zone-center phonon frequencies, despite the choice of the HSE parameters and the PAW potentials different from Wahl *et al.* The external strain u_{ext} is defined as $(a - a_0)/a_0$ using the theoretical stress-free a-axis lattice constant (a_0) of a tetragonal $BaTiO_3$ calculated with *each* XC functional.

III. GINZBURG-LANDAU (GL) THEORY AND EXPERIMENTS

The total energy of a ferroelectric phase at an electronic ground state is calculable, when the positions of all the nuclei are given, because the ground state electron density is calculable from these positions. For the ground state, this can also be done with the positions of a part of nuclei because the other nuclei positions can be obtained through the minimization of the total energy. For ferroelectricity, the effective choice of these nuclei positions is that contributing to the polar distortion, which is the basis of GL theory.

In the GL theory,[31–33] the change of free energy from that of the paraelectric phase is expressed by spontaneous polarization P_S and strain u that correspond, respectively, to polar and nonpolar distortions. The coefficients of this expression are chosen so that the measurables given by the GL energy agree with the experiments of a *specific sample* under study. Therefore, the coefficients depend on the samples of these experiments, and the GL coefficients of $BaTiO_3$ have changed substantially with years,[31,32,52,53] reflecting the increase of P_S and T_C by the improvements of crystal quality. This suggests that a GL theory can be regarded as a thermodynamic *description of representative samples*. Therefore, we may use GL results as semi-experimental data.

The standard GL theory appears slightly complicate[31,33] but becomes extremely simple, when restricted to cubic-tetragonal phase transition. When restricted to the tetragonal ($P4mm$) phase such as $BaTiO_3$ and $PbTiO_3$, the increase of T_C and P_S by in plane compressive stress is self-evident.[20,24] Therefore it has been known theoretically since the proposal of the GL theory by Devonshire,[31] and experimentally been proved since the 1970s.[16,35] We should be aware that mechanical stress or mechanical boundary condition in GL theory expresses only a part of epitaxial effect.

The present *ab initio* calculations are for the RT phase of $BaTiO_3$, which is experimentally unstable at 0 K under a stress-free condition. That is, the present *ab initio* calculations deduce the quantities, when this RT phase happens to exist at 0 K. Likewise, the GL theory below deduces the quantities, when this RT phase continues to exist down to 0 K. Hence, the comparisons of the quantities given by these two methods are meaningful, while the GL results are considered semi-experimental data.

The GL free energy of bulk ferroelectric having an m3m symmetry in a paraelectric phase is given as[31,33]

$$\begin{aligned}\Delta G(P,X) = {} & \alpha_1\left(P_1^2+P_2^2+P_3^2\right)+\alpha_{11}\left(P_1^4+P_2^4+P_3^4\right)+\alpha_{12}\left(P_1^2P_2^2+P_2^2P_3^2+P_3^2P_1^2\right)+\alpha_{111}\left(P_1^6+P_2^6+P_3^6\right)\\ & +\alpha_{112}\left[P_1^4\left(P_2^2+P_3^2\right)+P_2^4\left(P_3^2+P_1^2\right)+P_3^4\left(P_1^2+P_2^2\right)\right]+\alpha_{123}P_1^2P_2^2P_3^2\\ & -\frac{s_{11}}{2}\left(X_1^2+X_2^2+X_3^2\right)-s_{12}(X_1X_2+X_2X_3+X_3X_1)-\frac{s_{44}}{2}\left(X_4^2+X_5^2+X_6^2\right)-Q_{11}\left(X_1P_1^2+X_2P_2^2+X_3P_3^2\right)\\ & -Q_{12}\left[X_1\left(P_2^2+P_3^2\right)+X_2\left(P_1^2+P_3^2\right)+X_3\left(P_1^2+P_2^2\right)\right]-Q_{44}(X_4P_2P_3+X_5P_1P_3+X_6P_1P_2),\end{aligned} \tag{1'}$$

where the suffixes of polarization P 1, 2, and 3 represent x, y, and z component, where the z and x directions are along the c and a axis of the unit cell. The suffixes 1, 2, 3, 4, 5, and 6 of stress $\boldsymbol{X}$ in Voigt notation represent xx, yy, zz, yz, xz, and xy component.

Li *et al.* improved the first two lines of Eq. (1′) by taking up to the 8th power of P.[32] We substitute the first two lines of Eq. (1′) with the formula of Li *et al.* GL free energy for tetragonal symmetry per unit volume is derived from this modified Eq. (1′) by setting $P_3 = P$, $P_1 = P_2 = 0$, $X_1 = X_2 = X$, $X_4 = X_5$,

and $X_6 = 0$.

$$\Delta G(P,X) = \Delta G_0(P) - g(X) - Q_{11}X_3P^2 - 2Q_{12}XP^2, \quad (1)$$

$$\Delta G_0(P) = \alpha_1 P^2 + \alpha_{11}P^4 + \alpha_{111}P^6 + \alpha_{1111}P^8, \quad (1a)$$

$$\alpha_1 \equiv \frac{T - T_C}{2\varepsilon_0 C}, \quad (2)$$

$$g(X) \equiv \frac{s_{11}}{2}\left(2X^2 + X_3^2\right) + s_{12}\left(X^2 + 2XX_3\right) + s_{44}X_4^2. \quad (3)$$

Here, T, C, and ε_0 are ambient temperature, Curie constant, and vacuum permittivity, respectively. $G_0(P)$ in Eq. (1) is a GL energy for stress-free condition; α_1, α_{11}, α_{111}, and α_{1111} are the dielectric stiffness and higher order stiffness coefficients at constant stress; s_{ij} is the elastic compliance coefficient at constant polarization, and Q_{ij} is the cubic electrostrictive constant. Unlike ordinary GL expansions, Eq. (1) contains a P^8 term but is returned to common expressions[31,52] by using proper values for α_1, α_{11}, and α_{111} and setting $\alpha_{1111} = 0$.

When strain u is variable instead of stress X, the Legendre transformation yields

$$\begin{aligned}\Delta H(P,u) &= \Delta G(P,X) + 2Xu + X_3u_3 + 2X_4u_4,\\ &= \Delta G_0(P) - g(X) - Q_{11}X_3P^2 - 2Q_{12}XP^2\\ &\quad + 2Xu + X_3u_3 + 2X_4u_4. \end{aligned} \quad (4)$$

The strains at equilibrium are given by $\partial H/\partial X_3 = 0$, $\partial H/\partial X_4 = 0$, and $\partial H/\partial X = 0$, which yields $\partial G/\partial X_3 = -u_3$, $\partial G/\partial X_4 = -2u_4$, and $\partial G/\partial X = -2u$, which gives two equations for X and X_3,

$$X \equiv \frac{s_{11}u - s_{12}u_3 - (s_{11}Q_{12} - s_{12}Q_{11})P^2}{(s_{11} - s_{12})(s_{11} + 2s_{12})}, \quad (5a)$$

$$X_3 \equiv \frac{(s_{11} + s_{12})u_3 - 2s_{12}u - ((s_{11} + s_{12})Q_{11} - 2s_{12}Q_{12})P^2}{(s_{11} - s_{12})(s_{11} + 2s_{12})}. \quad (5b)$$

The stress-free condition $X = X_3 = 0$ yields spontaneous elastic strains $u_{sp3} = Q_{11}{P_S}^2$ and $u_{sp} = Q_{12}{P_S}^2$. Therefore, the lattice constants a and c of the stress-free tetragonal phase are

$$a = a_C\left(1 + u_{sp}\right) = a_C\left(1 + Q_{12}P_S^2\right), \quad (6a)$$

$$c = a_C\left(1 + u_{sp3}\right) = a_C\left(1 + Q_{11}P_S^2\right), \quad (6b)$$

where a_C is the lattice constant of the stress-free cubic phase at T_C.

For an in plane stress only case ($X_3 = X_4 = 0$), Eqs. (5a) and (5b) yield $X = (u - Q_{12}P^2)/(s_{11} + s_{12})$. By this equation, the stress and coupling terms in Eq. (4) are $\Delta H - \Delta G_0 = -(s_{11} + s_{12})X^2 - 2Q_{12}XP^2 + 2Xu = (u^2 - 2uQ_{12}P^2 + {Q_{12}}^2P^4)/(s_{11} + s_{12})$. When $\Delta H - \Delta G_0$ is expressed by this equation, Eq. (4) becomes

$$\Delta H(P,u) = \alpha_1^u P^2 + \alpha_{11}^u P^4 + \alpha_{111}P^6 + \alpha_{1111}P^8 + \frac{u^2}{s_{11} + s_{12}}, \quad (7)$$

$$\begin{aligned}\alpha_1^u &\equiv \frac{T - (T_C + \Delta T_C)}{2\varepsilon_0 C}\\ &= \frac{}{2\varepsilon_0 C}(T - (T_C + 4\varepsilon_0 C\frac{Q_{12}u}{s_{11} + s_{12}})),\end{aligned} \quad (7a)$$

$$\Delta T_C = 4\varepsilon_0 C\frac{Q_{12}u}{s_{11} + s_{12}}, \quad (7b)$$

$$\alpha_{11}^u \equiv \alpha_{11} + \frac{Q_{12}^2}{s_{11} + s_{12}}. \quad (7c)$$

The stress-free condition $X = 0$ is expressed by $\partial H^u/\partial u = 0$. This gives $-2Q_{12}P^2/(s_{11} + s_{12}) + 2u/(s_{11} + s_{12}) = 0$, yielding $u_{sp} = Q_{12}P^2$ again.

Equation (7a) shows the increase of T_c (ΔT_c) by in plane compressive stress, which indicates also an increase of P_S. This has been known over a half century because it is obvious from Eqs. (1)–(2)[20,24]

$$\begin{aligned}\Delta G(P,X) &= \Delta G_0(P) - g(X) - 2Q_{12}XP^2\\ &= \alpha_1' P^2 + \alpha_{11}P^4 + \alpha_{111}P^6 + \alpha_{1111}P^8 - g(X),\end{aligned} \quad (8)$$

$$\alpha_1' \equiv \frac{T - (T_C + \Delta T_C')}{2\varepsilon_0 C} = \frac{}{2\varepsilon_0 C}(T - (T_C + 4\varepsilon_0 C Q_{12}X)),$$

where $\Delta T_c' \equiv 4\varepsilon_0 C Q_{12}X$. Equation (8) becomes Eq. (7) by $X = (u - Q_{12}P^2)/(s_{11} + s_{12})$ derived for $X_3 = X_4 = 0$.

The equilibrium P_S is given by $\partial H^u/\partial P$ as

$$\alpha_1^u + 2\alpha_{11}^u P_S^2 + 3\alpha_{111}P_S^4 + 4\alpha_{1111}P_S^6 = 0. \quad (9)$$

When $\alpha_{1111} = 0$ as in the standard GL theories, Eq. (9) is solved easily. For $\alpha_{1111} \neq 0$, analytical solution is given by the Cardano formula for the cubic equation.

For $X_3 = 0$, Eq. (5b) gives $u_3 = 2s_{12}u/(s_{11} + s_{12}) + (Q_{11} - 2s_{12}Q_{12}/(s_{11} + s_{12}))P^2$. Consequently, the c-axis lattice constant c of a tetragonal phase with an external strain is given by

$$c_T = a_C\left(1 + \frac{2s_{12}u}{s_{11} + s_{12}} + (Q_{11} - \frac{2s_{12}Q_{12}}{s_{11} + s_{12}})P_S^2\right). \quad (10)$$

For stress-free case ($X = X_3 = 0$), the above relationship $u = u_{sp} = Q_{12}{P_S}^2$ is applicable, and therefore, Eq. (10) becomes Eq. (6b).

In the present *ab initio* calculations, the results are given for an external strain u_{ext}, which is the change from the a-lattice constant of the tetragonal $BaTiO_3$ under no external stress (a_0). On the other hand, the present GL theory gives the results for $u = u_{sp} + u_{ext}$. In Secs. IV–VI, the results are shown for u_{ext}. The constants in Eqs. (1)–(3) are the same throughout the present paper: $(2\varepsilon_0 C)^{-1} = 4.124 \times 10^5$ C^{-2} m^2 N/K, $\alpha_{11} = -2.097 \times 10^8$ C^{-4} m^6 N, $\alpha_{111} = 1.294 \times 10^9$ C^{-6} m^{10} N, and $\alpha_{1111} = 3.86 \times 10^{10}$ C^{-8} m^{14} N, and $Q_{12} = -0.044$ m^4 C^{-2}, $Q_{11} = 0.10$ m^4 C^{-22}, $s_{11} = 8.05 \times 10^{-12}$ m^2/N, and $s_{12} = -2.35 \times 10^{-12}$ m^2/N.[31,52–58]

In Fig. 1, the comparison of the present GL theory for the stress-free condition with experiments of $BaTiO_3$ demonstrates its validity. In Fig. 1(a), T_C in Eqs. (7a) and (9) is adapted from the experiment.[59] P_S by Eq. (9) agrees excellently with experimental P_S.[59–61] P_S of ideal samples can be higher than these experimental values, because a complete switching is difficult, especially at low T's,[60] and samples could be imperfect. Consequently, we cannot exclude the possibility that an appropriate P_S of the tetragonal phase at 0 K is slightly higher than the present GL estimations that are based on these experiments.

Figure 1(b) compares the T-dependence of the lattice constant by the GL theory with two experiments,[12,13] whereas the

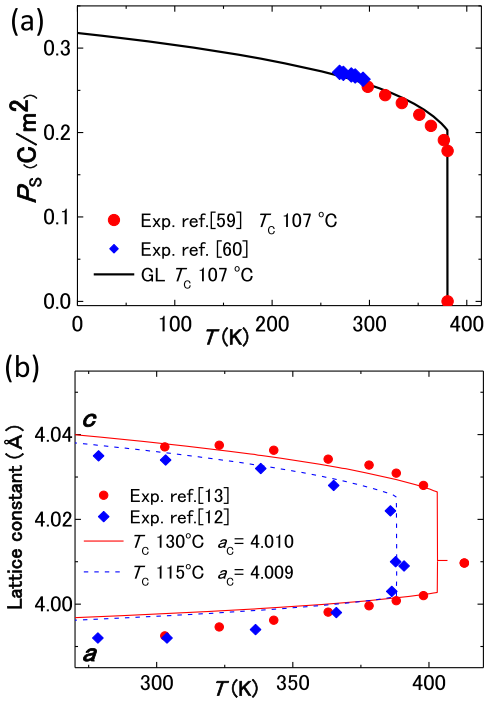

FIG. 1. Comparison of the present GL calculations of tetragonal $BaTiO_3$ with published experiments to examine the properties at 0 K (new criterion). (a) T-dependence of P_S.[59,60] T_C in the GL calculation is adapted from the experimental value of the curve (107 °C).[59] (b) T-dependence of the lattice constants of tetragonal phases a and c (Nakatani *et al.*,[13] Kay and Vousden[12]). T_C and a_C in the GL calculations are adapted from the experimental values of each curve.

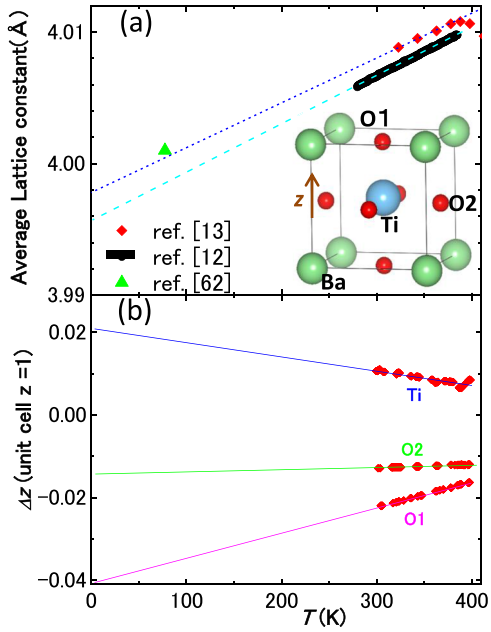

FIG. 2. (a) Experimental T-dependence of average lattice constant $V^{1/3} = (a^2c)^{1/3}$ and atomic positions of tetragonal $BaTiO_3$ red diamonds: Nakatani *et al.*,[13] black circles: Kay and Vousden,[12] green triangle: rhombohedral phase.[62] Dashed and dotted lines are linear fittings. (b) Experimental atomic positions expressed as atomic displacement of parallel to z axes from those of the cubic phase in fractions of the c lattice constant (Nakatani *et al.*,[13] Ba is at $z = 0$). Solid lines are linear fittings. In (a), the V data[13] at 298 K and 303 K are not plotted because they suffer a marked influence by the tetragonal-orthorhombic phase transition. The illustration of a $BaTiO_3$ unit cell defines the positions and symbols of specific atoms.

lattice constants are less sensitive to experimental difficulties than P_S. In Fig. 1(b), T_C and a_C in Eqs. (6a) and (6b) are those of each experiment. The a's and c's by the GL theory agree well with those of each experiment. Because the GL a's are larger than the experimental ones below RT and the GL c's are close to the experimental ones, Fig. 1(b) indicates that the GL volume V and GL c/a ratio at 0 K pose an *upper bound* of V and a *lower bound* of c/a at 0 K, respectively.

Kay and Vousden[12] showed that the average lattice constant changed linearly with T in all the phases of $BaTiO_3$: cubic, tetragonal, orthorhombic, and rhombohedral. Therefore, we use also a linear extrapolation of the experimental average lattice constant ($V^{1/3}$)[13] to 0 K in Fig. 2(a). This extrapolation is validated by an independent experiment of the rhombohedral phase[62] that is exactly on this extrapolation line.

The inset illustrates a $BaTiO_3$ unit cell and defines the positions of specific atoms. In particular, we denote an oxygen atom in a TiO_2 and BaO layer as O2 and O1, respectively. In Fig. 2(b), atomic displacements from cubic positions along the c-axis (Δz's) are plotted and extrapolated to 0 K. An appropriate Δz of each atom should be between Δz of each atom at RT and Δz of each atom extrapolated to 0 K because the change of lattice constants and atomic displacements should be slowing down below Debye temperature.[63,64]

Therefore, the extrapolations in Figs. 2(a) and 2(b) provide a lower bound of the unit cell volume V and an upper bound of $|\Delta z|$ of stress-free tetragonal $BaTiO_3$ at 0 K, whereas the data at RT provide an upper bound of V and a lower bound of $|\Delta z|$ at 0 K. A part of data in Figs. 1 and 2 is listed in Table I.

IV. STRESS-FREE TETRAGONAL $BaTiO_3$

A Hubbard-like potential U was tested for LDA+U, PBE+U, PBEsol+U, and TPSS+U with U = 0–8 eV applied to O_{2p} and Ti_{3d} states. Because TPSS+U with U = 8 eV on O_{2p} yielded the most appropriate c/a, V, and P_S in these tests, we show the results of this case. The choice of U = 8 eV on O_{2p} is consistent with the effectiveness of LDA+U and GGA+U with U on O_{2p} in Ti-containing oxides.[43,65]

In Fig. 3(a), the *ab initio* P_S and c/a in stress-free cases (u_{ext} = 0) are compared with experimental and GL data. The horizontal and vertical dashed-dotted lines represent the GL-P_S and GL-c/a at 0 K, respectively, whereas this c/a is a lower bound as discussed in Sec. III [Fig. 1(b)]. Therefore, the best *ab initio* estimate is the yellow shaded area on the horizontal line on the right-hand side of the vertical line. This shows that both P_S and c/a were underestimated by LDA and Wu-Cohen[9] but estimated appropriately by PBEsol, TPSS, TPSS+U, HSEsol, and B1-WC(PP).[10] [B1-WC(PP) stands for hybrid exchange-correlation functional by Bilc *et al.*[10] using the pseudopotential.] This rating is opposite to the conventional ones. Interestingly, all the P_S vs. c/a data are on a single curve, of which coefficient is given in Table II. In Fig. 3(a), the data of Wu-Cohen[9] represent approximately experimental P_S and c/a at RT, which is the conventional criterion.

TABLE I. Summary of present GL and *ab initio* results and published experimental data for tetragonal and stress-free cubic phase $BaTiO_3$. An experimental P_S is 0.269 C/m^2 at 270 K.[60] The experimental unit cell value at 0 K is from the extrapolation in Fig. 2(a). The value P_S by the GL theory is with T_C = 107 °C of the experiments in Fig. 2(a), whereas those in blanket are by the GL theory with T_C = 135 °C given by Ref. 13.

	u_{ext}	a (Å)	c (Å)	V (Å^3)	c/a	ΔTi	ΔO2	ΔO1	P_S(C m^{-2})	Eg (eV)
Expt. RT	0	3.993[a]	4.037[a]	64.35[a]	1.011[a]	0.010[a]	−0.013[a]	−0.022[a]	0.254[b]	3.27[c]
Expt. 403 K	0	4.010[a]								
Expt. 0 K	0			(63.89)	Extrapolation					
GL 298 K	0	3.998	4.038	64.54	1.010				0.257(0.267)	
GL 0 K	0	3.992	4.051	64.56	1.015				0.318(0.321)	
LDA										
	−0.020	3.862	4.114	61.36	1.065	0.018	−0.024	0.065	0.405	1.803
	−0.010	3.901	4.052	61.68	1.039	0.016	−0.018	0.039	0.339	1.777
	−0.005	3.921	4.025	61.88	1.027	0.015	−0.016	0.027	0.307	1.767
	0	3.941	3.990	61.97	1.012	0.013	−0.013	0.012	0.261	1.750
Cubic	0	3.949	3.949	61.60	1	0	0	0	0	
PBEsol										
	−0.020	3.892	4.192	63.50	1.077	0.018	−0.028	0.077	0.453	1.812
	−0.010	3.932	4.119	63.68	1.047	0.017	−0.022	0.047	0.385	1.775
	−0.005	3.952	4.086	63.81	1.034	0.016	−0.019	0.034	0.352	1.761
	0	3.971	4.059	64.01	1.022	0.016	−0.017	0.022	0.320	1.749
Cubic	0	3.986	3.986	63.31	1	0	0	0	0	
TPSS										
	−0.020	3.909	4.188	64.00	1.071	0.019	−0.027	0.071	0.434	1.843
	−0.010	3.949	4.141	64.59	1.049	0.018	−0.022	0.049	0.384	1.821
	−0.005	3.969	4.109	64.73	1.035	0.017	−0.020	0.035	0.355	1.807
	0	3.989	4.070	64.76	1.020	0.016	−0.017	0.020	0.318	1.794
Cubic	0	4.001	4.001	64.07	1	0	0	0	0	
TPSS+U										
	−0.020	3.891	4.190	63.45	1.077	0.019	−0.027	0.077	0.441	2.027
	−0.010	3.931	4.117	63.61	1.047	0.017	−0.021	0.047	0.376	1.981
	−0.005	3.951	4.088	63.81	1.035	0.017	−0.019	0.035	0.350	1.954
	0	3.971	4.045	63.77	1.019	0.015	−0.016	0.019	0.305	1.937
Cubic	0	3.982	3.982	63.13	1	0	0	0	0	
HSE										
	−0.0193	3.889	4.324	65.38	1.112	0.018	−0.038	0.112	0.550	3.428
	−0.0093	3.928	4.215	65.04	1.073	0.019	−0.029	0.073	0.472	3.372
	−0.0043	3.948	4.181	65.16	1.059	0.019	−0.026	0.059	0.449	3.358
	0	3.965	4.145	65.16	1.045	0.019	−0.024	0.045	0.421	3.348
	0.0050	3.985	4.112	65.31	1.032	0.018	−0.021	0.032	0.396	
Cubic	0	3.992	3.992	63.62	1	0	0	0	0	
HSEsol										
	−0.020	3.867	4.180	62.52	1.081	0.019	−0.027	0.081	0.452	3.404
	−0.010	3.907	4.100	62.58	1.049	0.018	−0.021	0.049	0.385	3.362
	−0.005	3.927	4.069	62.74	1.036	0.017	−0.019	0.036	0.358	3.335
	0	3.946	4.042	62.94	1.024	0.016	−0.017	0.024	0.333	3.307
Cubic	0	3.961	3.961	62.14	1	0	0	0	0	

[a]Experimental values: Ref. 13.
[b]Experimental values: Ref. 59.
[c]Experimental values: Ref. 89.

The appropriate values of V and the distance between Ti and O2 along the c-axis (Δz_{Ti-O2}) at 0 K are in the yellow shaded area surrounded by vertical and horizontal lines in Fig. 3(b). Here, the vertical and horizontal dashed lines represent an experimental V and Δz_{Ti-O2} at RT, respectively, as discussed in Fig. 2. The vertical and horizontal dotted lines show an extrapolation of experimental V and Δz_{Ti-O2} to 0 K, respectively, as discussed in Fig. 2.

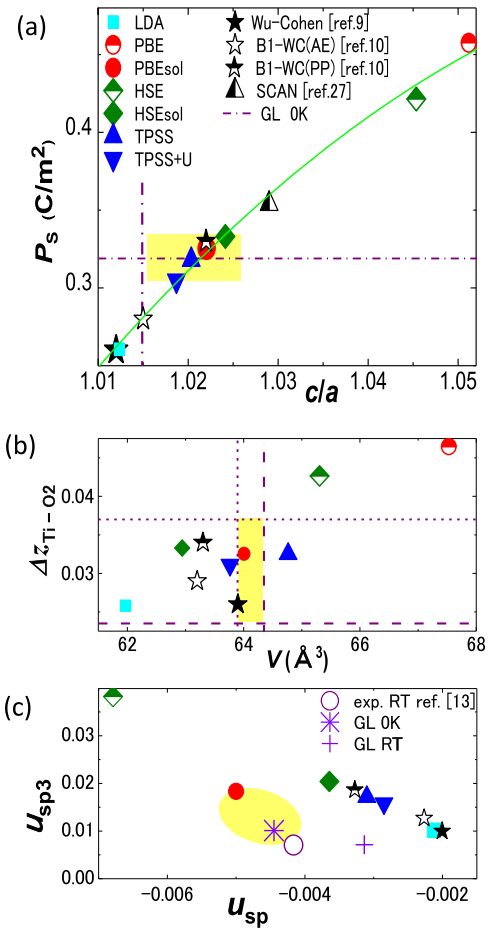

FIG. 3. Properties of *stress-free* tetragonal $BaTiO_3$ by the present and published *ab initio* calculations[9,10,26] compared with experiments and new criterion. Yellow shades show a plausible range. (a) P_S vs. *c*/*a*. The horizontal and vertical dashed-dotted lines show P_S and *c*/*a* at 0 K by the GL theory, respectively. The oblique solid lines are a fitting. (b) Distance of the Ti atom from the O atom along the *c*-axis (*z*-axis) in fractions of the *c* lattice constant (Δz_{Ti-O2}) vs. unit cell volume *V*. The dashed and dotted *vertical* lines represent an upper and a lower bound of *V*, respectively, which is given by the experiments at RT[13] and the extrapolations from Fig. 2(a). The dashed and dotted *horizontal* lines represent a lower and an upper bound of Δz_{Ti-O2}, respectively, which is given by the experiments at RT[13] and the extrapolations from Fig. 2(b). (c) In plane (u_{sp}) and out of plane (u_{sp3}) spontaneous strains. Asterisk, plus sign, and open circle represent GL results at 0 K and RT and an experimental data at RT, respectively. The values of data points and fitting parameters are listed in Tables I–III.

Consequently, PBSsol and TSSP+*U*, which predicted appropriate P_S and *c*/*a*, predicted appropriate *V* and Δz_{Ti-O2} at 0 K. The deviations of *V* and Δz_{Ti-O2} by the other XC functionals except for LDA, HSE, and PBE could be acceptable. *In brief, PBEsol and TPSS+U are considered to yield appropriate estimates of P_S, c/a, V, and Δz_{Ti-O2}.*

In addition, the in plane (u_{sp}) and out of plane (u_{sp3}) spontaneous strains calculated *ab initio* are plotted in Fig. 3(c). The experimental u_{sp3} is calculated from Ref. 13 by $(c_{298} - a_{413})/a_{413}$, where c_{298} and a_{413} are the *c* axis lattice constant at 298 K and the lattice constant of the cubic phase at 413 K, respectively. This poses a lower bound of u_{sp3} because the *c* lattice constant of the tetragonal phase tends to increase toward 0 K and the lattice constant of the cubic phase decreases toward 0 K. The comparison of the GL u_{sp} at 0 K and RT in Fig. 3(c) shows that $|u_{sp}|$ at 0 K is larger than $|u_{sp}|$ at RT. *Therefore, PBEsol and HSEsol are considered to predict appropriate values of u_{sp} and u_{sp3}.*

The *ab initio* calculations using experimental lattice constants may remedy the underestimations of lattice constants and P_S by LDA calculations. By using *a*- and *c*-lattice constants of $BaTiO_3$ at RT, we calculated P_S using LDA and PBEsol. These P_S's were much higher than the experimental value at RT (0.254 C/m^2 [59]), despite the use of RT lattice constants. This problem was severer with LDA ($P_S = 0.313$ C/m^2) than with PBEsol ($P_S = 0.303$ C/m^2). Similar overestimation of LDA was observed for $SrTiO_3$.[42]

The results of these *ab initio* calculations and those for cubic $BaTiO_3$ are summarized in Table I, which shows good agreement of the present LDA, PBE, PBEsol, and HSE results with previous calculations of stress-free $BaTiO_3$.[10,11,26,39] The fittings to these calculations are summarized in Table II. Table III lists elastic constants in addition to u_{sp} and u_{sp3} calculated from the *ab initio* *a*, *c*, and a_c. Table III lists also electrostrictive constants Q_{12} and Q_{11} given by these u_{sp} and u_{sp3} and the *ab initio* P_S through Eqs. (6a) and (6b). Most of the PBE and HSE results are not shown in Secs. V and VI because the results deviated unacceptably from experiments. The validity of the new criterion is confirmed in Sec. V.

V. TETRAGONAL $BaTiO_3$ UNDER EXTERNAL STRAIN

In the present paper, the external biaxial in plane strain $u_{ext} \equiv (a - a_0)/a_0$, where *a* and a_0 are the *a*-axis lattice constant under external stress and no external stress (stress-free), respectively, and are calculated *ab initio* with a same XC functional. For example, $u_{ext} = (a^{LDA} - {a_0}^{LDA})/{a_0}^{LDA}$ for LDA, and $u_{ext} = (a^{PBEsol} - {a_0}^{PBEsol})/{a_0}^{PBEsol}$ for PBEsol. The suffix 0 stands for no external stress. Similarly, $(c/a)/(c/a)_0$ is the ratio of *c*/*a* for $u_{ext} \neq 0$ to *c*/*a* for $u_{ext} = 0$ ($(c/a)_0$).

The lower bound of u_{ext} is −0.02, below which thin film growth without significant defects and dislocations is empirically unsuccessful. Although lattice constants are measured more reliably than P_S, they may still contain artifacts. For example, the *c*-lattice constant, the unit cell volume *V*, and *c*/*a* increase by off-stoichiometry.[66–71] This problem is severe for Si and Ge substrates because an insufficient oxidizing environment is used. These elongations of the *c*-lattice constant are due to a pure chemical origin and unrelated with ferroelectricity or the depolarization field because they occur in many nonferroelectric metal oxides.[66–71] On the other hand, the increase of *c*/*a* is reduced by dislocations, which tends to occur for large strain.[36,72,73] These data are removed or remarked in Figs. 4–6.

In Fig. 4, P_S increases with compressive strain in agreement with experiments[35,36,73–78] and the GL theories.[24,31] The present LDA results agree overall with the LDA results by Ederer.[39] In Fig. 4, for a small strain, the *ab initio* P_S agrees well with the GL P_S; but for a large strain, the *ab initio* P_S increases more rapidly than the GL P_S. This is because the coefficients in Eqs. (1)–(3) are obtained from experiments using small stress above RT. In particular, the appropriate elastic compliance coefficients s_{11} and s_{12} would be

TABLE II. Parameters of fittings to *ab initio* results. The value of parameter C is absent, when the fitting is linear. "O" and "O*" in the 1st column indicate that the fitting is forced to pass the origin (0, 0) and passes near the origin, respectively. R^2 and σ stand for the coefficient of determination and the standard deviation, respectively.

$y = A + Bx + Cx^2$	y	x	A	B	C	R^2	σ
Figure 3(a)	P_S (C/m^2)	c/a	−49.046 1	90.991 1	−41.7708	0.993	0.0059
Figure 4							
PBEsol	P_S (C/m^2)	u_{ext}	0.323 64	−6.285		−1.000	0.0019
TPSS+U			0.309 78	−6.652		−0.996	0.0061
HSEsol			0.329 38	−6.010		−0.997	0.0049
Figure 5(b)							
PBEsol	c/a	u_{ext}	1.020 94	−2.763		−0.999	0.0013
TPSS+U			1.019 21	−2.881		−0.999	0.0011
HSEsol			1.022 71	−2.853		−0.998	0.0018
Figure 5(c)	$c/a/(c/a)_0$	u_{ext}	0.999 955	−2.680		−0.997	0.0017
Figure 6(c)	Δz_{Ti-O}	u_{ext}	0.032 25	−0.696 2		−0.995	0.0006
	Δz_{Ti}	u_{ext}	0.015 90	−0.154 8		−0.931	0.0005
	Δz_O	u_{ext}	−0.016 35	0.541 6		0.992	0.0006
Figure 7(a)	P_S (C/m^2)	c/a	−1.991 01	2.263 21		0.996	0.0047
Figure 7(b)	P_S (C/m^2)	c (nm)	−3.186 49	0.867 18		0.976	0.01421
Figure 8(a) O	P_S (C/m^2)	Δz_{Ti}	3.236×10^{-5}	11.19	607	0.997	0.0098
Figure 8(b)	P_S (C/m^2)	Δz_{Ti-O1}	0.085 16	5.494		0.988	0.0101
O			9.791×10^{-5}	8.509	−25.6	0.999	0.0063
Figure 8(c) O*	P_S (C/m^2)	Δz_{Ti-O2}	3.55×10^{-4}	9.771		1.000	0.0045
Figure 8(d)	P_S (C/m^2)	Δz_{O2}	0.131 57	−11.53		−0.986	0.0109
O			1.272×10^{-4}	−22.80	−227	0.999	0.0050

lower than the present values (Table III) and are expected to decrease with u_{ext}.[79] This is supported by the underestimation of the c, c/a, and V under strain by the GL theory in Figs. 5 and 6.

The comparisons of the GL curves of P_S, c/a, $(c/a)/(c/a)_0$, and V at 0 K and 298 K in Figs. 4 and 5 indicate that the effect of biaxial strain surpasses the temperature effect for $u_{ext} < -0.01$. Therefore, as mentioned in Sec. I, the direct comparison of the *ab initio* P_S, c/a, V, and $(c/a)/(c/a)_0$ with the experimental ones at RT is meaningful for $u_{ext} < -0.01$. In Fig. 4, P_S's by all the calculations except for LDA and HSE are close to the experimental P_S at $u_{ext} \approx -0.022$.[78]

Although reliable experimental P_S's under strain are limited, c/a correlates well with P_S in Fig. 3(a) and the measurements of the lattice constants are more reliable than those of P_S. However, in Fig. 5(a) showing lattice constants vs u_{ext}, some thin film data (small open circles) show c-lattice constants larger than the other thin film data (open circles).[13,73–78] Because the data represented by these small open circles have the unit-cell volume appreciably larger than those of bulk single crystals, they appear substantially influenced by off-stoichiometry and are not displayed in the subsequent figures. *In this view, PBEsol, TPSS+U, and HSEsol are considered to agree with experimental c-lattice constants.*

The comparison of the GL results at 0 K and 298 K in Fig. 5(b) suggests that the experimental c/a at 298 K can represent approximately 0 K data when being shifted by the distance indicated by the arrows. The meaningful comparison with experiments is for $u_{ext} < -0.01$ (yellow shaded area), where RT effect is unimportant. Therefore, PBEsol, TPSS+U, HSEsol, and TPSS are considered to agree with experimental c/a.[73–76,78] In addition, the curves of $(c/a)/(c/a)_0$ vs. u_{ext} by all the *ab initio* calculations in Fig. 5(c) are fitted by a single line that agrees well with the experimental $(c/a)/(c/a)_0$.

Because unit cell volume V is $ca_0^2(1 + u_{ext})^2$, Fig. 5(a) suggests that PBEsol, TPSS+U, and HSEsol predict appropriate V's under strain. In Fig. 6(a), V calculated with all the *ab initio* calculations except for LDA are consistent with experiments.[73–76,78] In particular, PBEsol and TPSS+U agreed mutually. Consistently with the c vs. u_{ext} in Fig. 5(a), the unit cell volume by the GL theory in Sec. III decreased rapidly with u_{ext}, disagreeing with both experiments and *ab initio* calculations. This error can be resolved by the GL theory that uses *ab initio* P_S and electrostrictive coefficients in Table III.

In Eq. (7), the minimum of the P-dependent part of the GL free energy, which gives an equilibrium P_S for a given u [Eq. (9)], is negative and decreases with $|u|$. Therefore, the change of GL free energy ΔF in Fig. 6(b) should be dominated by the elastic term in Eq. (7): $u^2/(s_{11} + s_{12})$, which is consistent with the observation of $\Delta F \propto u_{ext}^2$ in the inset of Fig. 6(b). Therefore, ΔF by the GL

TABLE III. Spontaneous strains along the *a*-axis (u_{sp}) and *c*-axis (u_{sp3}) and electrostrictive coefficients Q_{11} and Q_{12} at 0 K deduced from *ab initio* *a*- and *c*-lattice constants and P_S through Eqs. (6a) and (6b) in comparison with experimental values at RT and values by the GL theory for RT and 0 K. Elastic compliances (GPa) of cubic and tetragonal $BaTiO_3$ calculated with PBEsol and HSEsol is listed.

	u_{sp}	u_{sp3}	Q_{12}	Q_{11}
LDA	−0.0021	0.010	−0.031	0.15
PBEsol	−0.0050	0.018	−0.047	0.17
TPSS	−0.0031	0.017	−0.031	0.17
TPSS+*U*	−0.0029	0.016	−0.031	0.17
HSE	−0.0068	0.038	−0.043	0.24
HSEsol	−0.0036	0.020	−0.033	0.18
Expt. RT	−0.0042[a]	0.007[a]	−0.044[b]	0.10[c] 0.11[b]
GL 0 K	−0.0045	0.010		
GL RT	−0.0031	0.007		

		C_{11}	C_{12}	C_{13}	C_{33}	C_{44}	C_{66}
Cubic	PBEsol	311	104			125	
Cubic	HSEsol	343	128			151	
Cubic	Expt.[b] ~410 K	164	67			108	
	Expt.[d] ~410 K	173	82				
Tetra	PBEsol	299	111	85	136	125	107
Tetra	HSEsol	324	126	97	152	143	131

[a]Experimental values: Ref. 13.
[b]Experimental values: Ref. 55.
[c]Experimental values: Ref. 54.
[d]Experimental values: Ref. 56.

theory, which was approximately 60% of the *ab initio* ΔF's, can be corrected by multiplying the literature value of $s_{11} + s_{12}$[55,56] with 0.6. This is consistent with the comparison of the experimental and *ab initio* elastic constant in Table III.

The *ab initio* ΔF exhibited also $\Delta F \propto u_{ext}^2$, confirming the dominance of elastic contribution to the strain-induced

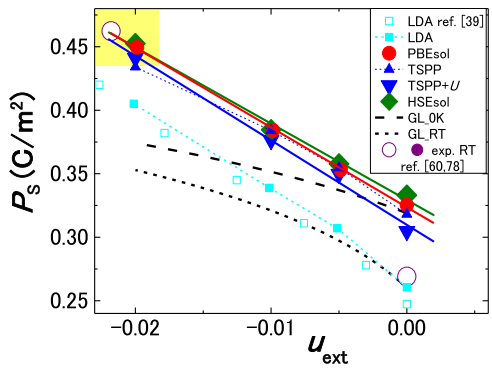

FIG. 4. External biaxial in plane strain (u_{ext}) dependence of P_S of tetragonal $BaTiO_3$, compared with experiments (open circles) at RT at $u_{ext} < 0$[78] and at 270 K at $u_{ext} = 0$.[60] Yellow shade shows a plausible range. Open squares show the published LDA results.[39] The dashed and dotted lines represent the GL results for 0 K and RT, respectively. The comparison of these two GL curves indicates an approximate amount of correction needed to convert RT data into 0 K data. Solid lines are a fitting to each result by PBEsol, TPSS+*U*, and HSEsol.

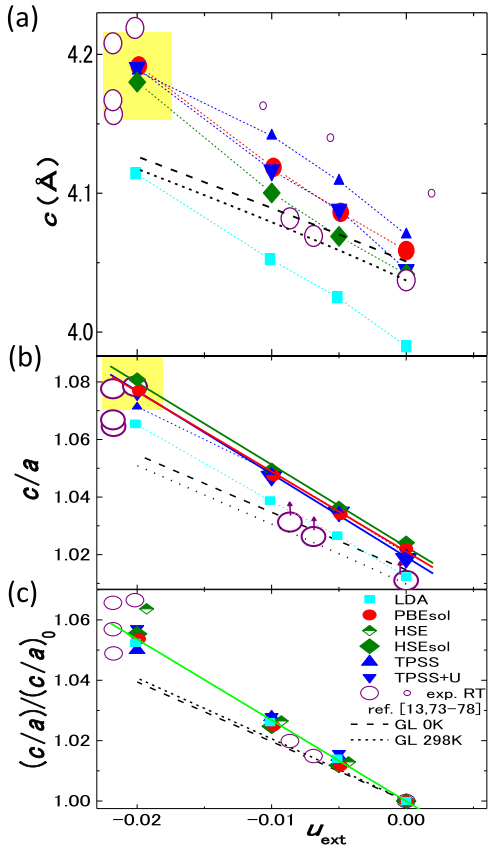

FIG. 5. u_{ext}-dependence of (a) *c*, (b) *c*/*a*, and (c) ratio of *c*/*a* to the stress-free *c*/*a* of tetragonal $BaTiO_3$, compared with thin film data[73–78] and a single crystal data at RT[13] (open circles and small open circles). Yellow shades show a plausible range. The dashed and dotted lines represent the GL results for 0 K and RT, respectively. The comparison of these two GL curves gives an approximate amount of correction needed to convert RT data into 0 K data, which is shown by arrows in (b). Solid lines in (b) are fittings to each result by PBEsol, TPSS+*U*, and HSEsol. In (a) and (b), HSE data are not displayed. The solid lines in (c) are the fitting to all the results except for those by HSE.

ΔF. This inference is reconfirmed by *ab initio* ΔF of $SrTiO_3$ that exhibited also $\Delta F \propto u_{ext}^2$ and had the values similar to those in Fig. 6(b) despite very different values of P_S.[42] In Fig. 6(a), *V*'s by LDA and TPSS change more than those calculated by other *ab initio* calculations, whereas ΔF's given by all the *ab initio* calculations are almost the same in Fig. 6(b).

The dependence of internal forces on XC functional is also evident in the atomic displacements in Fig. 6(c). The atomic displacements by all the *ab initio* calculations were mutually similar except for those by LDA. The displacements of LDA were smaller and changed faster with u_{ext} than others, which is considered as the origin of the small P_S and its rapid change of P_S with u_{ext} in Fig. 4.

In summary, the calculations of stress-free and stressed $BaTiO_3$ in Secs. IV and V show that PBEsol, TPSS+U, and HSEsol yielded mutually similar results and agreed with experiments. That is, these XC functionals yielded similar volume, lattice constants, atomic positions, and P_S, although their accuracies of bandgaps were very different. LDA appeared to underestimate the lattice constants, P_S, and internal forces.

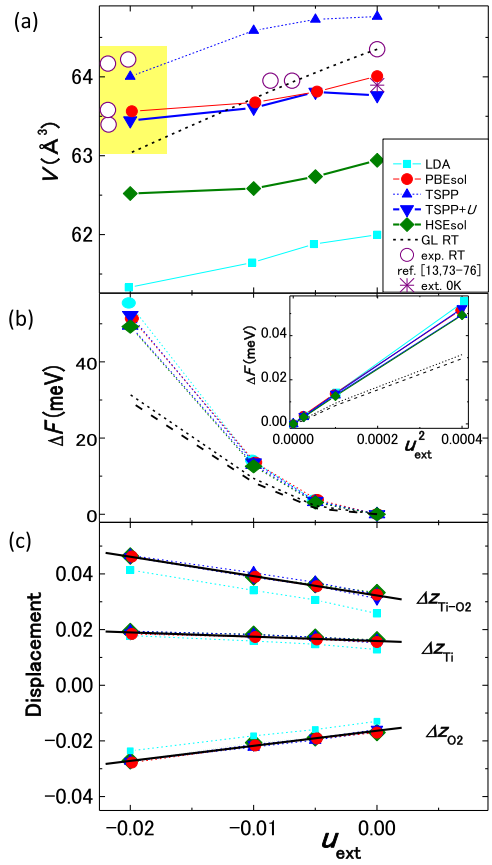

FIG. 6. (a) Unit cell volume V and (b) difference of free energy F from stress-free F (ΔF) are plotted against u_{ext}. (c) Displacements of Ti and O2 atoms from cubic positions along the c-axis (z-axis) (Δz_{Ti}, Δz_{O2}) and difference of them (Δz_{Ti-O2}) in fractions of the c lattice constant are plotted against u_{ext}. The inset shows the replot of ΔF as the functions of u_{ext}^2. Open circles in (a) are experimental volume of thin films[73–76] and a single crystal[13] at RT. The volume of a single crystal[13] extrapolated to 0 K is shown by an asterisk. Yellow shade shows a plausible range of values. The GL results used the experimental stress-free volume at RT.[13] In (a) and (b), the GL results for 0 K and RT are shown by the dashed and dotted lines, respectively. The solid lines in (c) are fittings to all the data except for LDA. Fitting parameters are listed in Table II.

VI. CRYSTALLOGRAPHIC ESTIMATION OF P_S

We found that the plot of P_S vs. certain crystallographic parameters under different strains calculated with several XC functionals lay precisely on a single curve, despite widely varying P_S. Thus, we think that the primary crystallographic origins of P_S can be found by a set of P_S and crystallographic parameters calculated *ab initio* with different XC functionals, which can be used for the crystallographic estimation of local P_S. An example is transmission electron microscopy (TEM), which uses frequently the displacement of the Ti atom from the center of the unit cell to identify P_S and its direction.[34]

The present Berry phase method for P_S[50,51] is considered accurate because the calculations with all the XC functionals for experimental ion positions and lattice constants at 303 K[13] agreed with the experimental P_S at 298 K (exp.: 0.25 C/m^2,[59,61] LDA, PBEsol, and TPSS+U: 0.24 C/m^2, and HSEsol: 0.23 C/m^2). In addition, P_S by different XC functionals was virtually the same for the crystallographic parameters given by PBEsol for stress-free $BaTiO_3$; LDA: 0.326 C/m^2, PBEsol: 0.325 C/m^2, TPSS: 0.326 C/m^2, TPSS +U: 0.323 C/m^2, HSE: 0.312 C/m^2, and HSEsol: 0.312 C/m^2. These calculations confirmed that ion positions determined P_S predominantly.

Therefore, the wide variations of the *ab initio* P_S in Secs. IV and V were mostly due to the difference of the estimation of the crystallographic parameters: lattice constants and ion positions. Here, each functional tended to yield specific deviations of crystallographic properties from ideal experimental ones. We think that such deviations exist locally in experiments owing to ambient temperature, defects, and local strains. Because of the correctness of the present Berry phase method,[50,51] the *ab initio* P_S *deviating from ideal experiments can be reinterpreted as exact calculations of* P_S *in crystals deviating from ideal ones.* That is, all the *ab initio* P_S's in Secs. IV and V correspond exactly to the experimental situations.

Consequently, the correlations between P_S and crystallographic properties calculated with different XC functionals (Figs. 7 and 8) correspond to those in experiments. Therefore, these correlations are used to identify the primary crystallographic property responsible for P_S that is usable for crystallographic identification of P_S in experiments. The parameters of fitting curves in Figs. 7 and 8 are summarized in Table II for the experimental estimation of P_S. All the nonlinear fittings passed the origin of each figure and the linear fitting in Fig. 8(c) passed the close vicinity of the origin.

In agreement with established knowledge, P_S correlated with c/a in Fig. 7(a). However, the c-lattice constant correlated with P_S better than c/a [Fig. 7(b)], which validates the

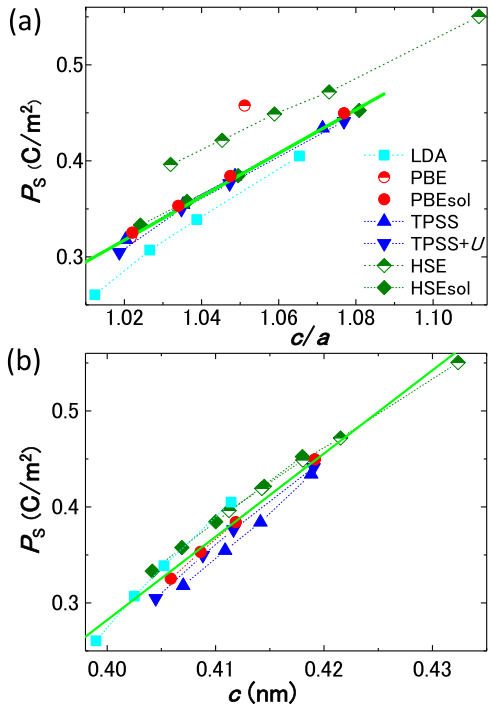

FIG. 7. (a) P_S vs. c/a and (b) P_S vs. c lattice constant for stress-free and strained tetragonal $BaTiO_3$. Solid lines are fittings, which are for the whole results by PBEsol, PBE, TPSS, TPSS+U, and HSEsol in (a) and for all the results in (b). Fitting parameters are listed in Table II.

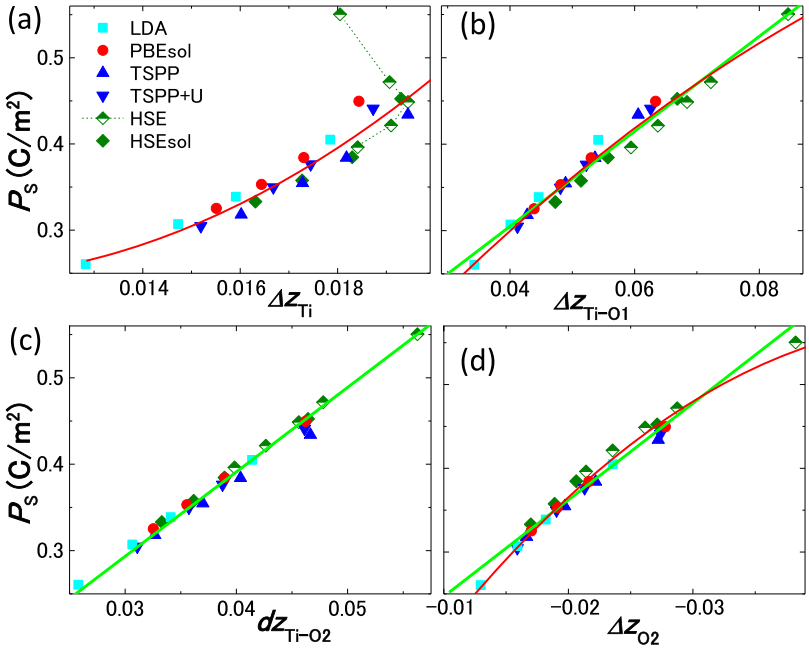

FIG. 8. Correlation of P_S with atomic displacements (a) Δz_{Ti}, (b) Δz_{Ti-O1}, (c) Δz_{Ti-O2}, and (d) Δz_{O2} of tetragonal $BaTiO_3$. The displacements are measured from the cubic position parallel to c-axes (z-axis) in fractions of the c lattice constant, and Δz_{Ti-O2} and Δz_{Ti-O1} are the difference between Δz_{Ti} and Δz_{O2} and between Δz_{Ti} and Δz_{O1}, respectively, and the Ba atom is at (0, 0, 0). Solid lines are linear and nonlinear fittings to all the results in each panel, except for those by HSE in (a). Fitting parameters are listed in Table III.

comparison of c-lattice constants in Fig. 5(a) as substitutes of P_S. In contrast to the conventional view, the correlation between P_S and the unit cell volume V was weak as indicated by Figs. 4 and 6(a). Therefore, the good correlation of the c-lattice constant with P_S is considered due to the combined effect of c/a and V. The conventional crystallographic identifier Δz_{Ti} (inset of Fig. 2) was found also to correlate with P_S, although some Δz_{Ti} results by HSE were out of correlation [Fig. 8(a)].

Both oxygen ion positions (Δz_{O1}, Δz_{O2}) correlated with P_S better than Δz_{Ti} [Figs. 8(b)–8(d)], although the values of the Born charges[10,26] suggest that their correlations be similar to that of Δz_{Ti}. Especially, the correction of Δz_{Ti-O2} and Δz_{O2} with P_S was excellent, whereas P_S depended linearly on Δz_{Ti-O2} and nonlinearly on Δz_{O2}. Therefore, both Δz_{O2} and Δz_{Ti-O2} are useful as identifiers of P_S, where the same conclusion holded for $SrTiO_3$.[42]

Because P_S correlates excellently with Δz_{O2} and Δz_{Ti-O2} and a substantial contribution to Δz_{Ti-O2} came from Δz_{O2}, the ferroelectricity of $BaTiO_3$ and $SrTiO_3$ is considered as oxygen-driven, as explained by Bilz *et al.*[80] In terms of $\Gamma 15$ zone-center phonon of the cubic lattice, the present displacement patterns were equal to a mixture of Slater, Last, and Axe modes,[81–83] whereas the weight of Slater mode was larger than others in $BaTiO_3$ and the weight of each mode was nearly the same in ferroelectricity in $SrTiO_3$.[42]

VII. IMPLICATIONS OF PRESENT RESULTS

In this section, we call the comparisons with the experiments at RT the *conventional criterion*, calling the comparisons with the GL theory results at 0 K presented above the *new criterion*. Here, P_S is the most essential criterion.

A. Published and present results

Many *ab initio* calculations of the bulk properties of prototypical ferroelectric $BaTiO_3$ have been reported[9,39,40] and examined in benchmark tests.[10,11,26,27] In the previous *ab initio* calculations of tetragonal $BaTiO_3$, the *conventional criterion* (stress-free) is used. For example, Wu-Cohen GGA XC functional,[9] which is the basis of B1-WC,[10] is considered accurate because it yields the properties that agree with the conventional criterion. Consequently, B1-WC(AE) in Table VI of Ref. 10 yields the properties that are consistent with the conventional criterion. [B1-WC(AE) stands for hybrid exchange-correlation functional by Bilc *et al.*[10] using the all-electron potential.] Moreover, the search for accurate XC functional for prototypical ferroelectrics including $BaTiO_3$ continues based on the conventional criterion until now.[26,27] An important target of these searches is the solution of the *super-tetragonality* (c/a) error and the resulting overestimation of P_S as written in the abstract of the recent paper.[26] Here, we confirmed that XC functionals were far more important for the accuracy than the parameters such as PAW potentials, k-point sampling, energy cutoff, convergence algorithms, the screening length in HSE, etc.

In the conventional criterion for stress-free $BaTiO_3$ (c/a = 1.01–1.011, P_S = 0.254 C/m^2, etc., Table I), PBE, PBEsol, TPSS, TPSS+U, HSE, HSEsol, B1-WC(PP),[10] SCAN,[26] and B3LYP[10] overestimated c/a and P_S [Fig. 3(a)]. These comparisons were partly reported by Wahl *et al.*[11] and Table IV of Bilc *et al.*[10] In this conventional criterion, LDA and Wu-Cohen[9] yielded accurate c/a and P_S of stress-free $BaTiO_3$, and B1-WC(AE)[10] yielded accurate P_S [Fig. 3(a), Table I].

The opposite conclusion was shown by the new criterion for stress-free $BaTiO_3$ (c/a = 1.015, P_S = 0.318 C/m^2, etc., Table I); TSSP and TSSP+U yielded accurate c/a and P_S, while LDA and Wu-Cohen[9] underestimated both c/a and P_S, and B1-WC(AE)[10] underestimated P_S [Fig. 3(a)]. Both c/a and P_S given by PBEsol, HSEsol, and B1-WC(PP)[10] were acceptable in the new criterion [Fig. 3(a)]. These conclusions agreed with those for the heavily strained cases in Figs. 4 and 5.

The present study aimed to find the approaches of *ab initio* calculations that yielded accurate predictions of

inhomogeneous ferroelectrics that have internal large strain and clarify the limitation of the accuracy. In particular, in Figs. 4 and 5, the experimental properties at large strain agree with the results by PBEsol, etc., and disagree with the results by LDA that have been used for strain dependence so far.[37–41] This suggests that the results for other ferroelectrics are also better to be reexamined with appropriate XC functionals.

Hybrid functionals estimated energy gap far better than DFT. Because the electron distribution is important for P_S, we were interested in the accuracy of P_S given by hybrid functionals (HSE, HSEsol). However, Figs. 3–5 show that improvements by hybrid functionals were not evident. Therefore, we can perform accurate calculation with less computation-demanding DFT, except for torsional distortion such as antiferro-distortive rotation of $SrTiO_3$.[42]

B. Depolarization instability, domain, size effect

The accuracy of P_S is the main factor for the accuracy of stability of ferroelectricity, which is critically important for domains,[1,18,20,34] depolarization field instability, and size effect.[19–21] The stability of stress-free ferroelectricity is the difference between free energy of ferroelectric and paraelectric phase $\Delta G_{f\text{-}p}$ or $\Delta H_{f\text{-}p}$. In Fig. 9, $\Delta G_{f\text{-}p}$ and $\Delta H_{f\text{-}p}$ given by *ab initio* and GL calculations decrease drastically with P_S.

The curves by GL theory in Fig. 9 are obtained in the following manner: $\Delta H - u^2/(s_{11} + s_{12})$ with $P = P_S$ in Eq. (7) gives $\Delta H_{f\text{-}p}$ because the free energy of the paraelectric phase ($P = 0$) is set to be zero. That is,

$$\Delta H_{f-p} = \alpha_1^u P_S^2 + \alpha_{11}^u P_S^4 + \alpha_{111} P_S^6 + \alpha_{1111} P_S^8. \quad (11)$$

$P = P_S$ satisfies Eq. (9). Using Eq. (9) with $P = P_S$, Eq. (11) is changed to

$$\Delta H_{f-p} = -\alpha_{11}^u P_S^4 - 2\alpha_{111} P_S^6 - 3\alpha_{1111} P_S^8. \quad (12)$$

Similarly, in the stress-free case, we obtain from Eq. (1a),

$$\Delta G_{f-p} = -\alpha_{11} P_{S0}^4 - 2\alpha_{111} P_{S0}^6 - 3\alpha_{1111} P_{S0}^8, \quad (13)$$

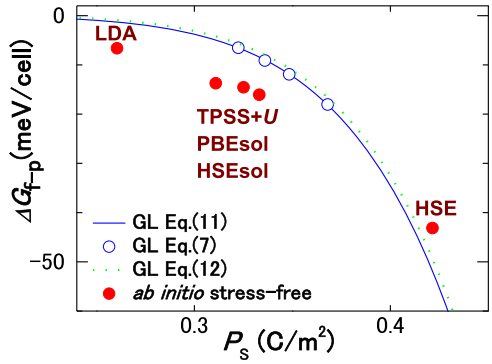

FIG. 9. $\Delta G_{f\text{-}p}$ ($\Delta H_{f\text{-}p}$) vs. P_S. Solid and dashed lines represent universal curves by GL theory using Eqs. (12) and (13), respectively. Filled and open circles represent *ab initio* calculations and GL calculations using Eq. (7), respectively.

where P_{S0} stands for P_S under stress-free condition. In addition, $\Delta H_{f\text{-}p}$ was obtained through the direct numerical minimization of Eq. (7), which should agree with Eq. (12).

Equations (12) and (13) show that $\Delta H_{f\text{-}p}$ and $\Delta G_{f\text{-}p}$ are functions of only P_S because all the coefficients in Eqs. (12) and (13) are constants (no u, no T). Therefore, we reinterpret that Eqs. (12) and (13) represent the universal P_S-dependence of free energy of tetragonal $BaTiO_3$ regardless of the origin of P_S change.

In the conventional theory for 1-dimensional cases, the depolarization field and its electrostatic energy density are approximately $-P_S/\varepsilon_0$ and $P_S^2/2\varepsilon_0$, respectively.[21,84] The sum of $P_S^2/2\varepsilon_0$ and $\Delta G_{f\text{-}p}$ ($\Delta E_{f\text{-}p}$) determines the existence or inexistence of ferroelectricity. In Fig. 9, despite only 20% difference of P_S, $\Delta G_{f\text{-}p}$ given by LDA is a half of $\Delta G_{f\text{-}p}$ given by TPSS+U, PBEsol, and HSEsol because $\Delta G_{f\text{-}p}$ depends critically on P_S. This shows the significance of the accuracy of P_S for the fundamental problem, e.g., the depolarization instability. In particular, Fig. 9 shows that LDA substantially underestimates the stability of ferroelectricity, whereas it has been used in most of calculations of depolarization instability and size effect.

In realistic treatment of the depolarization instability, the domain should be considered. In addition, the GL theory by Watanabe *et al.*[24,25,85] has predicted (1) existence of the *free carrier layer at polar discontinuities* (Fig. 10): ferroelectric/insulator interface, ferroelectric free-surface, and charged domain boundaries, (2) diminished depolarization instability and size effect by screening of these carriers, and, therefore, (3) freer domain configurations. The example of (3) is the stable existence of the domains in Fig. 10(a) even without defects, and the example of (2) is the stability of P_S in Fig. 10(b). In this theory, the accuracy of $P_S^2/2\varepsilon_0$ and $\Delta F_{f\text{-}p}$ is even more important than that in the aforementioned standard theory.

For the ferroelectric free-surface, the predictions (1) free carrier layer and (3) domains were experimentally verified with $BaTiO_3$,[25,85] which was confirmed by the *ab initio* calculations of Krčmar and Fu.[22] After these theory and experiments,[24,25] the conduction at $SrTiO_3/LaAlO_3$ was reported,[86] and its primary origin was recently found to be the depolarization field and defects.[87] Therefore, the results of $SrTiO_3/LaAlO_3$ verified partially the prediction (1) free carriers at the ferroelectric/insulator interface. In addition, another prediction of (1): free carriers at charged domain boundaries is reported recently in numerous publications.

The characteristics of prediction (2), which are recently called hyper-ferroelectricity, originate from the prediction (1). Therefore, all these issues will be clarified by the *ab initio* calculations of the prediction (1)[24,25] in an atomistic picture. In these calculations, the most important part is the shaded area of ferroelectric in Fig. 10(a)–10(c), where large strains and distortions exist. Because these strains and distortions in the shaded area are far larger than the RT effects, the XC functionals that agree with the new criterion will be effective. In addition, these XC functionals should be appropriate because these issues are interested as intrinsic ground state properties that are not due to the electron excitations from defects by a finite temperature.[24,25,85]

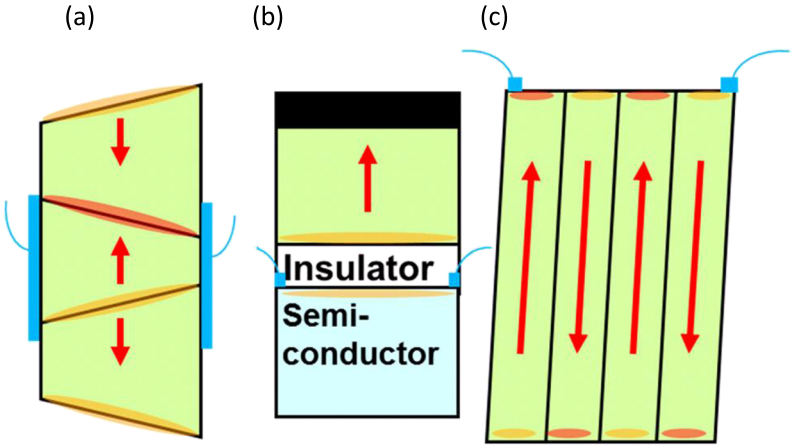

FIG. 10. Typical situations of free carrier layer formation at polar discontinuities by the depolarization field, where arrows and shades show P_S of the ferroelectric and carrier layer, respectively (adapted from Fig. 1 of Ref. 25): (a) head-to-head or tail-to-tail domain boundaries, (b) ferroelectric/insulator interface, (c) clean damage-free surface as a prototype. (b) and (c) were predicted by Ref. 24. (c) was experimentally verified in Refs. 25 and 85. These experiments and the theory[24] led to the generalization that includes (a).[25] The theoretical calculation[22,25] showed the thickness of the layer was approximately 1–3 nm, which was later experimentally confirmed by $SrTiO_3/LaAlO_3$.[86]

VIII. SUMMARY

The present paper proposed a new criterion for the accuracy of *ab initio* calculations of ferroelectrics under high strain and a method for obtaining the criterion that is the stress-free bulk properties at 0 K estimated by a GL theory. This criterion revealed the rating of the accuracy of *ab initio* calculations of tetragonal $BaTiO_3$ different from the conventional criterion, and the super-tetragonality error for tetragonal $BaTiO_3$ is much less than conventionally thought (Fig. 3). Here, strains are essential in many situations including inhomogeneous ferroelectric, e.g., domains and surface (Fig. 10), and the present paper showed more enhanced ferroelectricity by large strain than the previous reports in a definite manner.

To date, the comparisons of *ab initio* calculations with experiments on stress-free $BaTiO_3$ at RT have been used as the conventional criterion in benchmark tests,[10,11,26,27] demonstrating the effectiveness of LDA, Wu-Cohen,[9] and B1-WC(AE),[10] over other XC functionals. Because the comparison of *ab initio* calculations with properties at RT is undesirable, we proposed a new criterion, which is given by Ginzburg-Landau (GL) thermodynamics that can impose the same constraints on lattice symmetry as those of *ab initio* calculations, and is a thermodynamic *representation of experiments*. Therefore, to compare experiments with *ab initio* calculations that yield properties at 0 K, the present paper estimated experimental properties at 0 K using the GL theory in Sec. III. Using this new criterion, the present study examined LDA, PBEsol, TSSP+U, TSSP, HSE, and HSEsol,[4–10] where the Hubbard-like term U was 8 eV on oxygen atoms.[43,65]

The GL theory was also used to estimate an approximate magnitude of the temperature effect (the change in properties associated with the change in temperature from 0 K to RT). This showed that for an external strain $u_{ext} < -0.01$, the strain effect surpasses the effects of a temperature difference of 300 K, allowing for the direct comparison of *ab initio* results with experiments. This implies an effective $T_C \gg 300$ K for $u_{ext} < -0.01$ in Eqs. (7) and (7a). This was supported by our simple estimations of the effective T_C[88] that was >1100–1300 K for $u_{ext} < -0.01$ (except for LDA), whereas Eq. (7b) predicted 800 K at $u_{ext} = -0.01$.

In the new criterion (*stress-free*) for $BaTiO_3$, TSSP, and B1-WC(PP),[10] and, especially, HSEsol, PBEsol, and TSSP+U calculations of *both* P_S and crystallographic properties agreed with the experiments better than LDA, Wu-Cohen,[9] and B1-WC(AE),[10] in contrast to conventional views[10,11,26,27] (Secs. IV and V). In addition, the crystallographic properties *under stress* calculated with PBEsol, TSSP+U, and HSEsol were also consistent with the experiments. Consequently, the XC functionals that agreed with the new criterion agree with experiments under large strain, which confirms the reliability and generality of the new criterion. Therefore, $BaTiO_3$ under large stress or electric field that exceeds the RT effect can be calculated accurately with these XC functionals. The accuracy of Wu-Cohen,[9] B1-WC(AE) and B1-WC(PP),[10] and SCAN[26] for large strain on $BaTiO_3$ is expected to be similar to those estimated by the new criterion in Fig. 3.

Consistent with previous studies,[10,11,26,27] the agreement of LDA with experiments of stress-free $BaTiO_3$ at RT was excellent, particularly, with respect to the main properties of ferroelectricity: P_S, c/a, Δz_{Ti}, Δz_{O2}, and Δz_{O1}. This was due to the compensation of the temperature effect by the error of LDA since, in Figs. 4 and 5, the difference between the quantities obtained using LDA and others XC functionals (excluding HSE) was the same as the difference between the quantities using the GL theory for RT and 0 K. However, the agreement of the LDA calculation with experiments at RT is not expected in complex situations, such as domains and depolarization, because the large strain effects surpassed the effect of 300 K for $u_{ext} < -0.01$. For example, in Figs. 5(a) and 5(b), the strained experiments at RT agreed more with the other XC functionals (excluding HSE) than LDA for $u_{ext} < -0.01$. In general, XC functionals that are optimized for the conventional criterion will be effective for bulk $BaTiO_3$ at RT without large stress or electric field but will not be when the effects of stress or electric field surpass the RT effect. In addition, LDA overestimated P_S more than PBEsol, when experimental stress-free lattice constants were used.

For *cubic* $BaTiO_3$, the PBEsol, TSSP+U, and HSE approaches yielded mutually similar results and were consistent with experiments (Table I). Thus, both good and bad predictors of bandgaps worked well for P_S, c/a, Δz_{Ti}, Δz_{O2}, Δz_{O1}, and V of tetragonal and cubic $BaTiO_3$. Therefore, the

electronic states at the valence band maximum and conduction band minimum were not critical for most ferroelectric properties. In addition, the contribution of polar distortion, i.e., P_S-related distortion, to the change of the free energy due to the strain was much smaller than the contribution of the elastic energy [Sec. V, Fig. 6(b)]. The free energies and unit cell volumes suggest that the elastic compliance coefficients at 0 K for $u_{ext} < -0.01$ are lower by approximately 40% than experimental values at $u_{ext} \sim 0$,[55,56] which explains the difference between some properties obtained by the *ab initio* calculations and the GL theory.

The data points of P_S vs. certain crystallographic parameters under different strains calculated with different XC functionals were found to lie precisely on a single curve, despite the wide variations of these data points. Here, the present wide variation of P_S obtained by XC functionals was due to the variation of crystallographic parameters. Because such variations of crystallographic parameters are expected to exist locally in experiments, the parameters' theoretical variations were regarded as the experimental ones. These considerations have yielded empirical analytical expressions of P_S by crystallographic parameters.

The parameters that correlated best with P_S were Δz_{O2} and Δz_{Ti-O2}. This supports oxygen-driven ferroelectricity,[80] and Δz_{O2} and Δz_{Ti-O2} can be used as experimental identifiers of P_S, e.g., for TEM. In addition, the c-lattice constant correlated well with P_S, probably because it represented the combined effects of the c/a ratio and the volume. These results also suggest that the effectiveness of XC functionals for P_S can be measured by the correct prediction of Δz_{Ti-O2}, Δz_{O2}, or Δz_{O1} at zero-stress, or, approximately, c lattice constant or c/a ratio with volume at zero-stress. The present results and the related data in the literature are summarized in Tables I–III.

The present approach can also be useful for other ferroelectrics, when experiments using high quality samples that are the bases of GL theories are reported. As for $PbTiO_3$, the lattice constants near 0 K are experimentally known, but experimental P_S at RT (~0.75 C/m^2) is compared with *ab initio* calculations[10] because P_S near 0 K is experimentally unknown. Our GL theory estimate of P_S at 0 K is 0.84 C/m^2. This may be much lower than the intrinsic value because the development of high quality $PbTiO_3$ single crystals is still underway.

ACKNOWLEDGMENTS

The author acknowledges useful discussions with Dr. Masao Arai at NIMS, Dr. P. Erhart at Chalmers, Dr. G. A. Rossetti, Jr. at Connecticut, Dr. M. Iwata at Nagoya, Dr. P. Bloechl at Clausthal, and support from JSPS KAKENHI Grant No. JP26600087.

[1] M. E. Lines and A. M. Glass, *Principles and Applications of Ferroelectric and Related Materials* (Oxford University Press, Oxford, 1977).
[2] W. Kohn and L. J. Sham, Phys. Rev. **140**, A1133 (1965).
[3] J. P. Perdew, K. Burke, and M. Ernzerhof, Phys. Rev. Lett. **77**, 3865 (1996).
[4] J. P. Perdew *et al.*, Phys. Rev. Lett. **100**, 136406 (2008).
[5] J. Tao, J. P. Perdew, V. N. Staroverov, and G. E. Scuseria, Phys. Rev. Lett. **91**, 146401 (2003).
[6] J. Sun, M. Marsman, G. I. Csonka, A. Ruzsinszky, P. Hao, Y.-S. Kim, G. Kresse, and J. P. Perdew, Phys. Rev. B **84**, 035117 (2011).
[7] J. Heyd, G. E. Scuseria, and M. Ernzerhof, J. Chem. Phys. **118**, 8207 (2003).
[8] L. Schimka, J. Harl, and G. Kresse, J. Chem. Phys. **134**, 024116 (2011).
[9] Z. Wu and R. E. Cohen, Phys. Rev. B **73**, 235116 (2006).
[10] D. I. Bilc, R. Orlando, R. Shaltaf, G.-M. Rignanese, J. Íñiguez, and P. Ghosez, Phys. Rev. B **77**, 165107 (2008).
[11] R. Wahl, D. Vogtenhuber, and G. Kresse, Phys. Rev. B **78**, 104116 (2008).
[12] H. F. Kay and P. Vousden, Philos. Mag. **40**, 1019 (1949).
[13] T. Nakatani *et al.*, Acta Cryst. **72**, 151–159 (2016).
[14] K. A. Müller and H. Burkard, Phys. Rev. B **19**, 3593 (1979).
[15] F. W. Lytle, J. Appl. Phys. **35**, 2212 (1964).
[16] H. Uwe and T. Sakudo, Phys. Rev. B **13**, 271 (1976).
[17] J. G. Bednorz and K. A. Muller, Phys. Rev. Lett. **52**, 2289 (1984).
[18] Y. Watanabe, Ferroelectrics **401**, 61 (2010).
[19] I. P. Batra, P. Wurfel, and B. D. Silverman, Phys. Rev. B **8**, 3257 (1973).
[20] Y. Watanabe, J. Appl. Phys. **83**, 2179 (1998); Erratum, **84**, 3428 (1998).
[21] Y. Watanabe, Ferroelectrics **461**, 38 (2014).
[22] M. Krčmar and C. L. Fu, Phys. Rev. B **68**, 115404 (2003).
[23] R. E. Cohen, Ferroelectrics **194**, 323 (1997).
[24] Y. Watanabe, Phys. Rev. B **57**, 789 (1998).
[25] Y. Watanabe, M. Okano, and A. Masuda, Phys. Rev. Lett. **86**, 332 (2001).
[26] Y. Zhang, J. Sun, J. P. Perdew, and X. Wu, Phys. Rev. B **96**, 035143 (2017).
[27] J. Sun *et al.*, Nat. Chem. **8**, 831 (2016); A. Paul, J. Sun, J. P. Perdew, and U. V. Waghmare, Phys. Rev. B **95**, 054111 (2017).
[28] H. Sharma, J. Kreisel, and P. Ghosez, Phys. Rev. B **90**, 214102 (2014).
[29] Y. Watanabe, Phys. Rev. B **57**, R5563 (1998).
[30] Y. Watanabe, Phys. Rev. B **59**, 11257 (1999).
[31] A. F. Devonshire, Philos. Mag. **40**, 1040 (1949).
[32] Y. L. Li, L. E. Cross, and L. Q. Chen, J. Appl. Phys. **98**, 064101 (2005).
[33] M. J. Haun, E. Furman, S. J. Jang, H. A. McKinstry, and L. E. Cross, J. Appl. Phys. **62**, 3331 (1987).
[34] J. M. Gregg, Ferroelectrics **433**, 74 (2012).
[35] N. Yanase, K. Abe, N. Fukushima, and T. Kawakubo, Jpn. J. Appl. Phys., Part 1 **33**, 5305 (1999).
[36] Y. Watanabe, Y. Matsumoto, H. Kunitomo, M. Tanamura, and E. Nishimoto, Jpn. J. Appl. Phys., Part 1 **33**, 5182 (1994).
[37] T. Schimizu and T. Kawakubo, Jpn. J. Appl. Phys., Part 2 **37**, L235 (1998).
[38] T. Hashimoto *et al.*, Jpn. J. Appl. Phys., Part 1 **44**, 7134 (2005).
[39] C. Ederer and N. A. Spaldin, Phys. Rev. Lett. **95**, 257601 (2005).
[40] O. Diéguez, K. M. Rabe, and D. Vanderbilt, Phys. Rev. B **72**, 144101 (2005); H. N. Lee *et al.*, Phys. Rev. Lett. **98**, 217602 (2007).
[41] P. V. Ong and J. Lee, J. Appl. Phys. **112**, 014109 (2012); L. Ni *et al.*, Phys. B **406**, 4145 (2011).
[42] Y. Watanabe, "Semiferroelectric ground state of $SrTiO_3$ explaining symmetry induced ferroelectricity and conductivity at insulator interface, surface, impurities and domain boundaries" (unpublished).
[43] P. Erhart, A. Klein, D. Åberg, and B. Sadigh, Phys. Rev. B **90**, 035204 (2014).
[44] J. Paier *et al.*, J. Chem. Phys. **125**, 249901 (2006).
[45] A. I. Liechtenstein, V. I. Anisimov, and J. Zaanen, Phys. Rev. B **52**, R5467 (1995).
[46] S. L. Dudarev, G. A. Botton, S. Y. Savrasov, C. J. Humphreys, and A. P. Sutton, Phys. Rev. B **57**, 1505 (1998).
[47] P. E. Blöchl, Phys. Rev. B **50**, 17953 (1994).
[48] G. Kresse and J. Hafner, Phys. Rev. B **47**, 558 (1993); G. Kresse and J. Furthmüller, Comput. Mater. Sci. **6**, 15 (1996); Phys. Rev. B **54**, 11169 (1996); G. Kresse and D. Joubert, *ibid.* **59**, 1758 (1999).
[49] H. J. Monkhorst and J. D. Pack, Phys. Rev. B **13**, 5188 (1976).
[50] R. D. King-Smith and D. Vanderbilt, Phys. Rev. B **47**, 1651 (1993); D. Vanderbilt and R. D. King-Smith, *ibid.* **48**, 4442 (1993).
[51] R. Resta, Ferroelectrtics **136**, 51 (1992); Rev. Mod. Phys. **66**, 899 (1994).
[52] A. J. Bell, J. Appl. Phys. **89**, 3907 (2001).
[53] W. R. Buessem, L. E. Cross, and A. K. Goswami, J. Am. Ceram. Soc. **49**, 33 (1966).
[54] T. Yamada, J. Appl. Phys. **43**, 328 (1972).
[55] F. Jona and G. Shirane, *Ferroelectric Crystals* (Pergamon, New York, 1962).
[56] D. Berlincourt and H. Jaffe, Phys. Rev. **111**, 143 (1958).
[57] J. J. Wang, F. Y. Meng, X. Q. Ma, M. X. Xu, and L. Q. Chen, J. Appl. Phys. **108**, 034107 (2010).
[58] S. Piskunov, E. Heifets, R. I. Eglitis, and G. Borstel, Comput. Mater. Sci. **29**, 165 (2004).
[59] W. Merz, Phys. Rev. **91**, 513 (1953).
[60] H. H. Wieder, Phys. Rev. **99**, 1161 (1955).
[61] S. H. Wemple, M. Didomenico, Jr., and I. Camlibel, J. Phys. Chem. Solids **29**, 1797 (1968).
[62] A. W. Hewat, Ferroelectrtics **6**, 215 (1973).

[63]N. W. Ashcroft and N. D. Mermin, *Solid State Physics* (Saunders College Publishing, Philadelphia, 1976). See especially p. 494 for Grüneisen parameters.
[64]*Materials at Low Temperatures*, edited by R. P. Reed and A. F. Clark (American Society for Metals, Metal Park, 1983).
[65]M. E. Arroyo-de Dompablo, A. Morales-García, and M. Taravillo, J. Chem. Phys. **135**, 054503 (2011).
[66]M. Hiratani, Y. Tarutani, T. Fukazawa, M. Okamoto, and K. Takagi, Thin Solid Films **227**, 100 (1993).
[67]M. Hiratani, K. Imagawa, and K. Takagi, Jpn. J. Appl. Phys., Part 1 **34**, 254 (1995).
[68]A. Tsuzuki, K. Kato, K. Kusumoto, and Y. Torii, J. Mater. Sci. Lett. **16**, 1652 (1997).
[69]K. Morito, T. Suzuki, and M. Fujimoto, Jpn. J. Appl. Phys., Part 1 **40**, 1310 (2001).
[70]T. Ohnishi, M. Lippmaa, T. Yamamoto, S. Meguro, and H. Koinuma, Appl. Phys. Lett. **87**, 241919 (2005).
[71]C. M. Brooks *et al.*, Appl. Phys. Lett. **94**, 162905 (2009).
[72]E. Chernova *et al.*, Appl. Phys. Lett. **106**, 192903 (2015).
[73]H. Terauchi *et al.*, J. Phys. Soc. Jpn. **61**, 2194 (1992).
[74]H. Shigetani *et al.*, J. Appl. Phys. **81**, 693 (1997).
[75]T. Zhao, F. Chen, H. Lu, G. Yang, and Z. Chen, J. Appl. Phys. **87**, 7442 (2000).
[76]K. J. Choi *et al.*, Science **306**, 1005 (2004).
[77]O. Trithaveesak, J. Schubert, and C. Buchal, J. Appl. Phys. **98**, 114101 (2005).
[78]A. Petraru *et al.*, J. Appl. Phys. **101**, 114106 (2007). In Fig. 4, the value of $P_S = 0.462$ C/m^2 is obtained from the original P_S-E curve of a 30-nm-thick film by shifting the horizontal axis to compensate the bias field.
[79]A. Tröster *et al.*, Phys. Rev. B **95**, 064111 (2017).
[80]H. Bilz, G. Benedek, and A. Bussmann-Holder, Phys. Rev. B **35**, 4840 (1987).
[81]J. T. Last, Phys. Rev. **105**, 1740 (1957).
[82]J. C. Slater, Phys. Rev. **78**, 748 (1950).
[83]J. D. Axe, Phys. Rev. **157**, 429 (1967).
[84]For example, Y. Watanabe, in *Ferroelectric Thin Films*, edited by Y. Ishibashi and M. Okuyama (Springer, Tokyo, 2005), Vol. 177; *Ferroics and Multiferroics*, edited by H. Singh and W. Kleemann (Trans Tech., Zurich, 2012), Vol. 57.
[85]Y. Watanabe and D. Sawamura, Jpn. J. Appl. Phys., Part 1 **36**, 6162 (1997); Y. Watanabe and A. Masuda, *ibid.* **40**, 5610 (2001); Y. Watanabe, Ferroelectrics **333**, 57 (2006); Y. Watanabe, D. Matsumoto, Y. Urakami, T. Arai, A. Masuda, and S. W. Cheong, *ibid.* **367**, 23 (2008).
[86]A. Ohtomo and H. Y. Hwang, Nature **427**, 423 (2004).
[87] S. A. Pauli *et al.*, Phys. Rev. Lett. **106**, 036101 (2011); W. Siemons *et al.*, *ibid.* **98**, 196802 (2007); L. Iglesias, A. Sarantopoulos, C. Magén, and F. Rivadulla, Phys. Rev. B **95**, 165138 (2017); A. Savoia *et al.*, *ibid.* **80**, 075110 (2009).
[88]We obtained $\alpha_1{}^u$ through the substitution of *ab initio* P_S into Eq. (9) and substituted this $\alpha_1{}^u$ into (7a) with $T = 0$ to obtain an effective T_C $T_C{}^{eff} = T_C + \Delta T_c$,

$$T_C^{eff} = \varepsilon_0 C(4(\alpha_{11} + \frac{Q_{12}^2}{s_{11}+s_{12}})P_{Sinitio}^2 + 6\alpha_{111}P_{Sinitio}^2 + 8\alpha_{1111}P_{Sinitio}^6),$$

where $P_{Sinitio}$ is P_S given by an *ab initio* calculation and T in all coefficients of Eq. (7a) and this equation should be set 0 K because $P_{Sinitio}$ is for 0 K. For better calculations, the coefficients α should be those under strain. When the 8th power of P is absent as in usual GL equation such as Eq. (1′), $\alpha_{1111} = 0$.
[89]S. H. Wemple, Phys. Rev. B **2**, 2679 (1970).